Electronic Supplementary Material (ESI) for Materials Chemistry Frontiers.

Supporting Information

Comprehensive Understanding of Structure-Stacking-Property Correlation to Achieve High-performance Ternary Data-Storage Device

Qi-jian Zhang,[*,a] *Huan Cao,*[b] *Jun-yu Shen,*[*,a] *and Yang Li*[*,c] *and Jian-mei Lu*[b]

a School of Materials Engineering, Changshu Institute of Technology, Changshu, Jiangsu 215500, P. R. China

b College of Chemistry, Chemical Engineering and Materials Science, Soochow University, Suzhou, Jiangsu 215123, P. R. China

c Jiangsu Key Laboratory of Micro and Nano Heat Fluid Flow Technology and Energy Application, School of Physical Science and Technology, Suzhou University of Science and Technology, Suzhou, Jiangsu 215009, China

E-mail: flashright@163.com (Q.Z)

1. Materials

naphthalen-2-amine (special caution: this compound is a potent carcinogen and when we did the synthesis experiment, we have done enough protective measures, such as wore antigas mask and gloves and handle this material in the hood, in a word, avoid any skin contact), 4-bromobenzaldehyde, 2-octanone, 2-aminobenzenethiol, bis(pinacolato)diboron and other solvents were all purchased from Shanghai Energy Chemical Co., Ltd. China.

2. Experimental Section

2-(4-bromophenyl)benzo[d]thiazole (1). 2-aminobenzenethiol (5.0 g, 40.0 mmol) and 4-bromobenzaldehyde (7.4 g, 40.0 mmol) were dissolved in 50 mL DMSO and the reaction mixture was stirred at 100°C for 5 h. After completion of the reaction, the reaction mixture was diluted with H_2O and extracted with EtOAc (3 × 50 mL). The combined organic layer was washed with brine and dried over anhydrous sodium sulfate and then the organic solvents were completely removed by rotary evaporation. The residue was purified by column chromatography using petroleum ether/ethylacetate (3/1; v/v) as eluent to give **1** (10.4 g, 90%) as a white solid. ^{1}H NMR (400 MHz, $CDCl_3$, δ): 8.10 (d, *J* = 7.9 Hz, 1H), 8.02 – 7.96 (m, 2H), 7.92 (dd, *J* = 8.0, 0.5 Hz, 1H), 7.69 – 7.60 (m, 2H), 7.55 – 7.51 (m, 1H), 7.45 – 7.40 (m, 1H).

2-(4-(4,4,5,5-tetramethyl-1,3,2-dioxaborolan-2-yl)phenyl)benzo[d]thiazole (2). A mixture of compound **1** (10.0 g, 34.5 mmol), bis(pinacolato)diboron (8.8 g, 34.5 mmol), potassium acetate (6.7 g, 69.0 mmol) and Pd(dppf)Cl_2 (0.5 g, 0.7 mmol) were dissolved in 50 mL dioxane and heated to 80°C for 3 h under nitrogen atmosphere. After completion of the reaction, the reaction mixture was cooled to room temperature and mixed with 100 mL water. The organic phase was separated and aqueous phase was extracted with EtOAc (3 × 50 mL). The combined organic layers were dried over anhydrous sodium sulfate and evaporated to remove the solvents under vacuum. The residue was purified by column chromatography using petroleum ether/ethylacetate (3/1; v/v) as eluent to offer compound **2**

(8.1 g, 70%) as a white solid. ^{1}H NMR (400 MHz, $CDCl_3$, δ): 8.21 – 8.06 (m, 3H), 8.00 – 7.88 (m, 3H), 7.61 – 7.47 (m, 1H), 7.46 – 7.39 (m, 1H), 1.40 (s, 12H).

Compounds **3** and **4** were synthesized according to the methods described in literature.[1]

3-(4-bromophenyl)-1-hexylbenzo[f]quinoline (3). Yeild (1.3 g) 30%, white solid. ^{1}H NMR (400 MHz, DMSO-d_6, δ): 8.71 (s, 1H), 8.30 (s, 2H), 8.17 – 8.09 (m, 3H), 7.99 – 7.95 (m, 1H), 7.72 – 7.76 (m, 4H), 3.49 (t, *J* = 7.2 Hz, 2H), 1.87 – 1.80 (m, 2H), 1.57 – 1.46 (m, 2H), 1.41 – 1.20 (m, 4H), 0.88 (t, *J* = 7.0 Hz, 3H).

3-(3-bromophenyl)-1-hexylbenzo[f]quinoline (4). Yeild (1.5 g) 35%, white solid. ^{1}H NMR (400 MHz, DMSO-d_6, δ): 8.70 (d, *J* = 8.3 Hz, 1H), 8.52 (s, 1H), 8.33 (d, *J* = 7.5 Hz, 1H), 8.19 (s, 1H), 8.09 (t, *J* = 8.7 Hz, 2H), 7.97 (d, *J* = 8.9 Hz, 1H), 7.78 – 7.67 (m, 3H), 7.52 (t, *J* = 7.8 Hz, 1H), 3.65 – 3.42 (m, 2H), 1.86 (s, 2H), 1.64 – 1.41 (m, 2H), 1.38 – 1.27 (m, 4H), 0.87 (t, *J* = 6.8 Hz, 3H).

2-(4'-(1-hexylbenzo[f]quinolin-3-yl)-[1,1'-biphenyl]-4-yl)benzo[d]thiazole (p-BQBTZ). A mixture of compound **2** (0.4 g, 1.2 mmol), compound **3** (0.5 g, 1.2 mmol), $Pd(PPh_3)_4$ (41.6 mg, 0.04 mmol), K_2CO_3 (0.5 g, 3.6 mmol), H_2O (5 mL) and 30 mL dioxane were stirred for 5 h under nitrogen at 80°C. After completion of the reaction, the reaction mixture was diluted with H_2O and extracted with DCM (3 × 20 mL). The combined organic layer was washed with brine and dried over anhydrous sodium sulfate and then the organic solvents were completely removed by rotary evaporation. The residue was purified by column chromatography using petroleum ether/ethylacetate (3/1; v/v) as eluent to give ***p*-BQBTZ** (0.4 g, 65%) as a pale-yellow solid. ^{1}H NMR (400 MHz, $CDCl_3$, δ): 8.71 (d, *J* = 8.0 Hz, 1H), 8.36 (d, *J* = 7.8 Hz, 2H), 8.21 (d, *J* = 8.0 Hz, 2H), 8.11 (d, *J* = 8.2 Hz, 1H), 8.06 – 7.96 (m, 2H), 7.93 (d, *J* = 9.7 Hz, 2H), 7.87 – 7.82 (m, 4H), 7.69 (t, *J* = 8.3 Hz, 2H), 7.52 (t, *J* = 7.5 Hz, 1H), 7.41 (t, *J* = 7.4 Hz, 1H), 7.26 (s, 1H), 3.54 (t, *J* = 7.2 Hz, 2H), 2.06 – 1.94 (m, 2H), 1.64 – 1.59 (m, 2H), 1.49 – 1.32 (m, 4H), 0.94 (t, *J* = 6.8 Hz, 3H); ^{13}C NMR (300 MHz, $CDCl_3$, δ): 167.6, 154.6, 154.2, 150.3, 149.9, 143.0, 140.6, 138.6, 135.0, 132.9, 132.6, 131.1, 130.2, 129.6, 129.1, 128.0, 127.9, 127.5, 127.4, 127.3, 126.4, 126.3, 125.2, 124.2, 123.2, 121.6, 121.3, 38.1, 31.6, 29.8, 29.5, 22.6, 14.1; IR (KBr): *v* = 3052, 2923, 2855, 1580, 1545, 1478, 1451, 1400, 1355, 1312, 1252, 966, 825, 756, 744 cm^{-1}. Elemental Analysis: Calcd for C38H32N2S: C, 83.17; H, 5.88; N, 5.11. Found: C, 83.13; H, 5.82; N, 5.00.

2-(3'-(1-hexylbenzo[f]quinolin-3-yl)-[1,1'-biphenyl]-4-yl)benzo[d]thiazole (m-BQBTZ). Using a similar procedure for ***p*-BQBTZ**, resulting in ***m*-BQBTZ** (0.3 g, 50%) as pale-yellow solid. ^{1}H NMR (400 MHz, $CDCl_3$, δ): 8.72 (d, *J* = 8.5 Hz, 1H), 8.53 (s, 1H), 8.23 (d, *J* = 6.8 Hz, 3H), 8.11 (d, *J* = 7.6 Hz, 1H), 8.03 – 7.98 (m, 2H), 7.97 – 7.87 (m, 4H), 7.78 (d, *J* = 7.8 Hz, 1H), 7.74 – 7.63 (m, 3H), 7.52 (t, *J* = 7.6 Hz, 1H), 7.41 (t, *J* = 7.7 Hz, 1H), 7.26 (s, 1H), 3.55 (t, *J* = 8.0 Hz, 2H), 2.04 – 1.96 (m, 2H), 1.69 – 1.55 (m, 2H), 1.47 – 1.36 (m, 4H), 0.94 (t, *J* = 7.2 Hz, 3H); ^{13}C NMR (300 MHz, $CDCl_3$, δ): 167.7, 155.0, 154.2, 150.0, 149.8, 143.6, 140.7, 139.7, 135.0, 132.9, 132.6, 131.2, 130.1, 129.4, 129.1, 128.0, 127.8, 127.3, 127.0, 126.4, 126.3, 125.2, 124.3, 123.2, 121.6, 38.1, 31.6, 29.8, 29.5, 22.6, 14.1; IR (KBr): v = 3443, 3053, 2949, 2923, 2865, 1580, 1550, 1475, 1453, 1434, 1401, 1340, 1312, 1254, 1230, 1200, 1117, 968, 840, 752, 697 cm^{-1}. Elemental Analysis: Calcd for C38H32N2S: C, 83.17; H, 5.88; N, 5.11; S, 5.84. Found: C, 83.08; H, 5.85; N, 5.02.

3. Results and Discussion

3.1. Electrochemical properties

Generally speaking, the EHOMO and ELUMO energy levels can be estimated from the following two ways: one is to be calculated from the optical bandgap of the compounds by the following equation: EHOMO = $-[E_{ox}(\text{onset}) + 4.8 - E_{\text{Ferrocene}}]$; ELUMO^1= $E_{\text{HOMO}} + E_g$, where E_{ox}(onset) is the onset oxidation potential; the other is to be calculated from the first reduction wave of the CV data: EHOMO = $-[E_{ox}(\text{onset}) + 4.8 - E_{\text{Ferrocene}}]$; ELUMO^2 = $-[E_{red}(\text{onset}) + 4.8 - E_{\text{Ferrocene}}]$, and the detailed results of *p*-**BQBTZ** and *m*-**BQBTZ** compounds were listed in Table S1. As we can see, the ELUMO energy levels of these two methods showed a big difference, thus, the DFT calculation was simulated to determine which result is more suitable for *p*-**BQBTZ** and *m*-**BQBTZ** compounds, and the calculated results were also summarized in Table S1. Through the comparison, the calculation from the onset oxidation potential E_{ox}(onset) and the optical bandgap of the compounds (E_g) is more suitable for *p*-**BQBTZ** and *m*-**BQBTZ** compounds in this work.

3.2. Surface Morphologies

To investigate the surface morphology of ***p*-BQBTZ** and ***m*-BQBTZ** based thin films, atomic force microscopy (AFM) was used. As shown in Figure S20a, the AFM topography images clearly show that ***p*-BQBTZ** formed a continuous morphology in the film with the room-meat-square (RMS) roughness of 3.2 nm. However, the morphology of ***m*-BQBTZ** was obviously discontinuous, and the room-meat-square (RMS) roughness was nearly twice of ***p*-BQBTZ** based film (6.7 nm, Figure S20b). Although the lower RMS roughness offers a stronger guarantee for the effective connection between the ***p*-BQBTZ** film and the electrodes, the defects in ***p*-BQBTZ** and ***m*-BQBTZ** based films could act as charge trapping sites to limit the mobility of charge carriers.

4. Supporting Figures

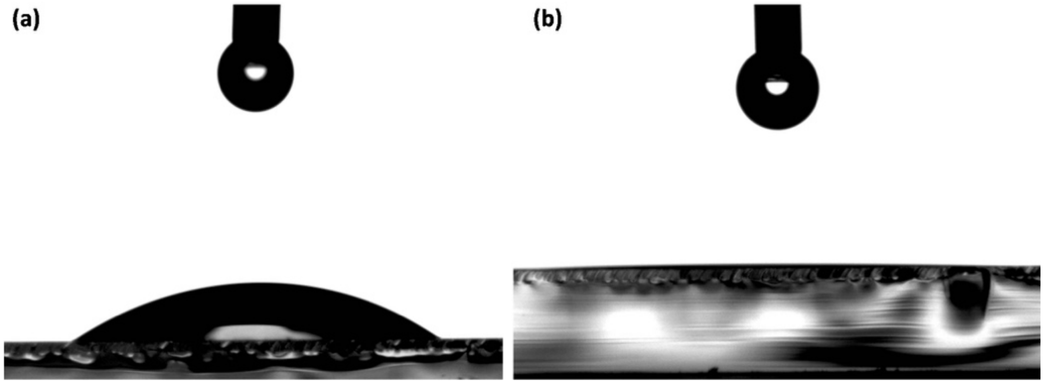

Figure S1. The contact angle tests of the ITO glass substrates before (a) and after (b) oxygen plasma treatment.

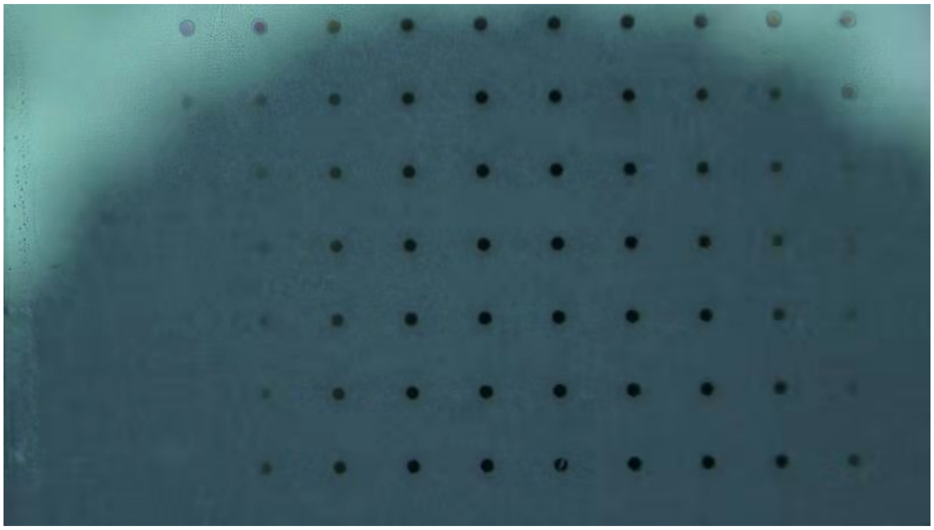

Figure S2. The active device area was about 0.0314 mm^2 using microscope.

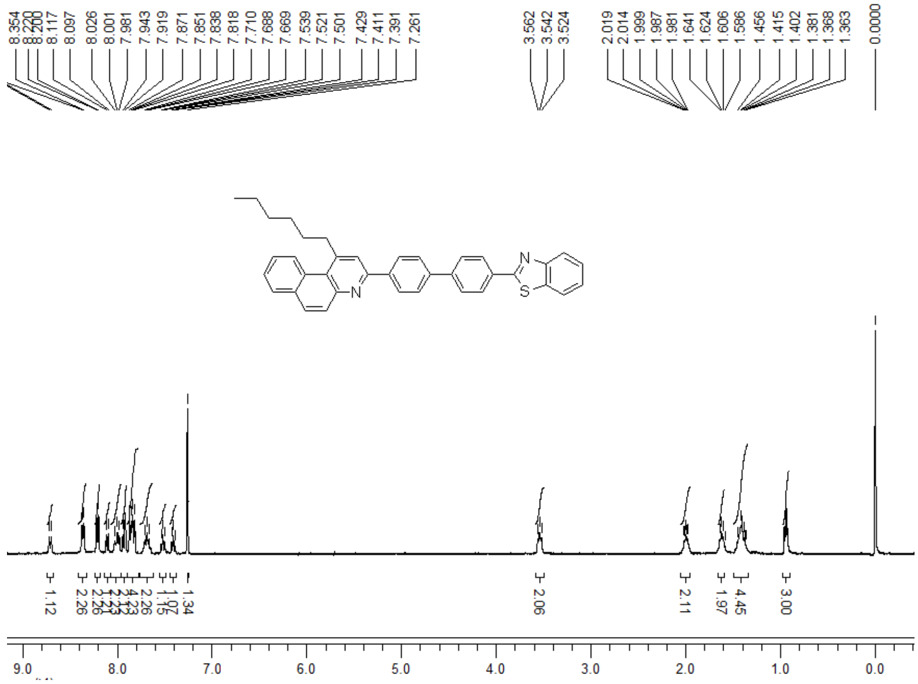

Figure S3. ^1H NMR spectra of ***p*-BQBTZ**.

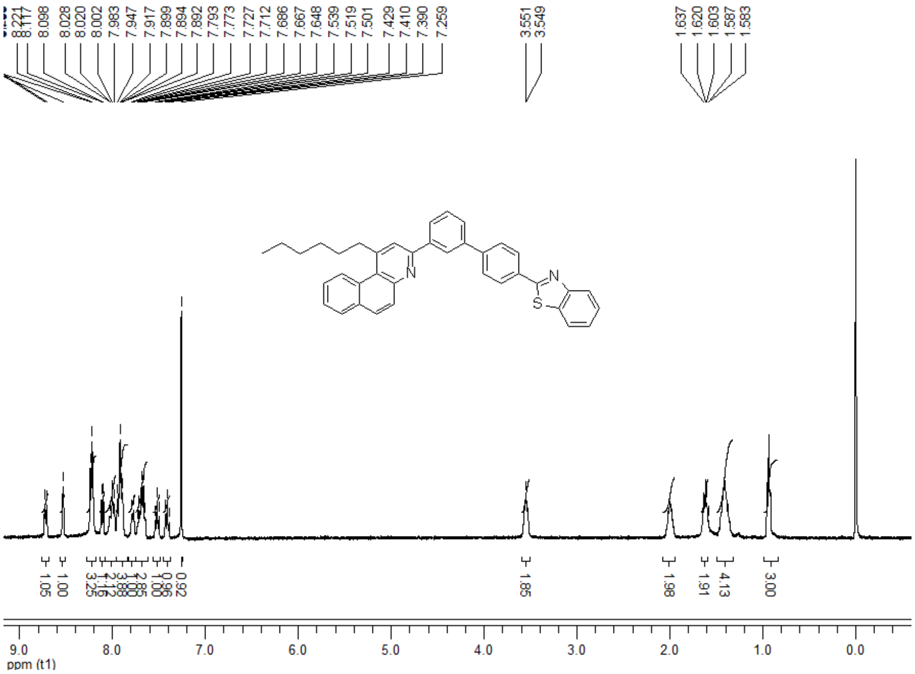

Figure S4. ^{1}H NMR spectra of ***m*-BQBTZ**.

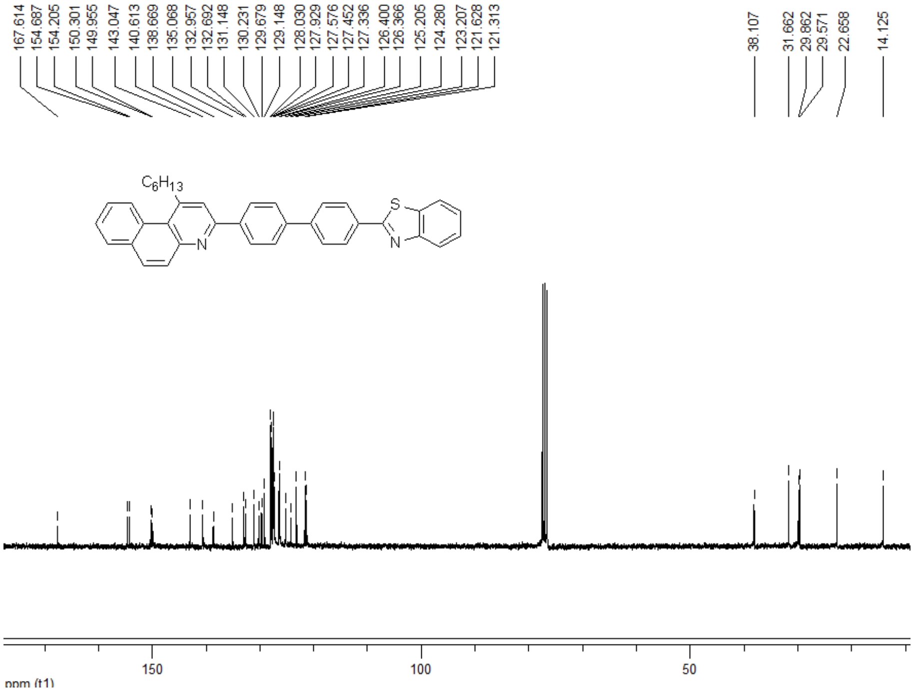

Figure S5. ^{13}C NMR spectra of ***p*-BQBTZ**.

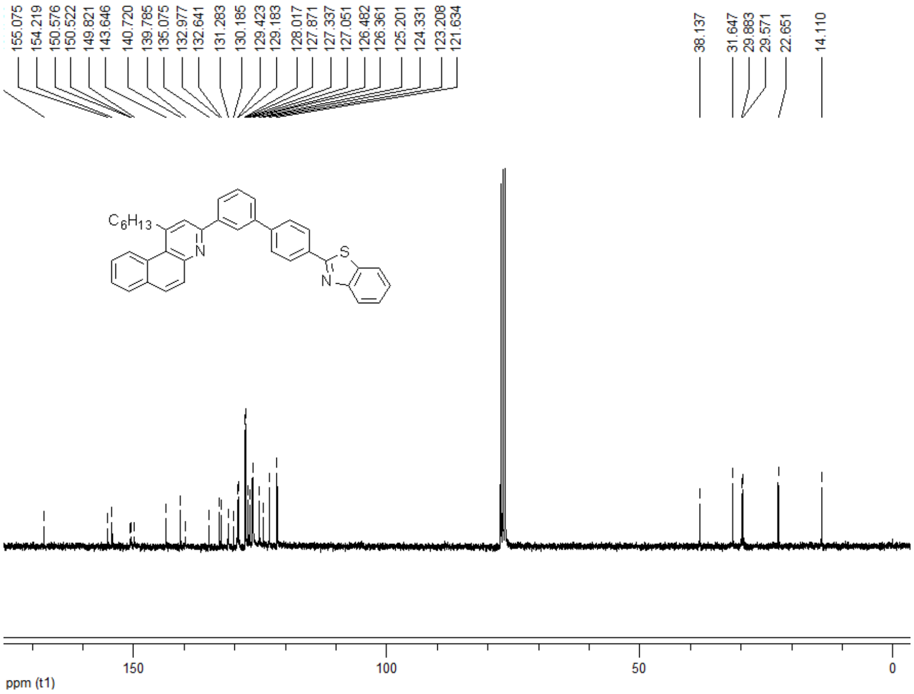

Figure S6. ^{13}C NMR spectra of ***p*-BQBTZ**.

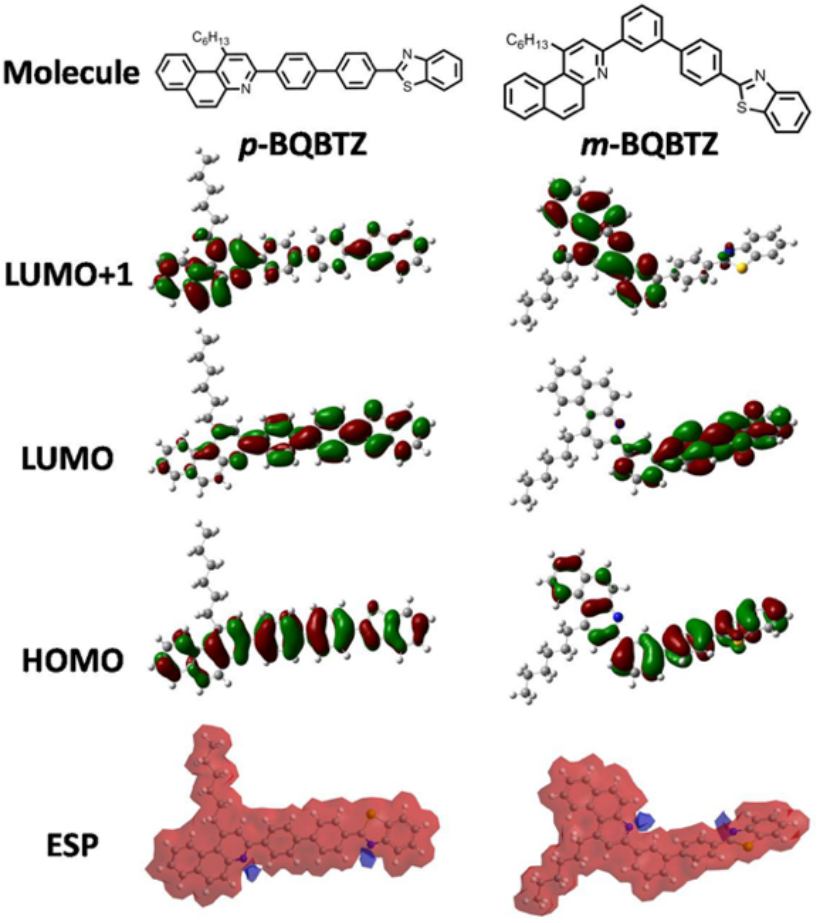

Figure S7. DFT molecular simulation results (B3LYP/6-311G (d) level) of ***p*-BQBTZ** and ***m*-BQBTZ**: molecular optimized geometry, ESP, HOMO and LUMO molecular orbitals.

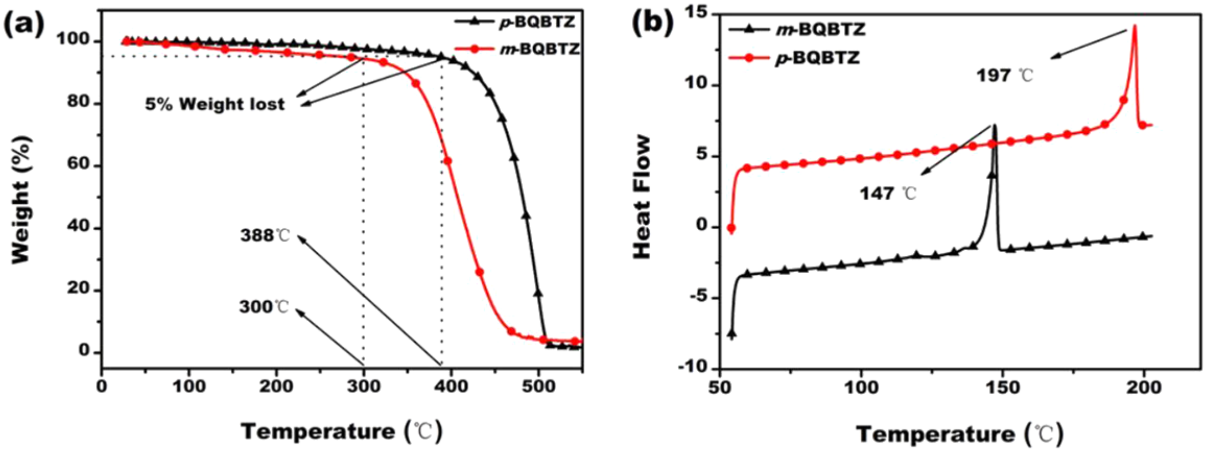

Figure S8. (a) TGA curves of ***p*-BQBTZ** and ***m*-BQBTZ** measured in nitrogen atmosphere at a heating rate of 10°C/min. (b) DSC plots for ***p*-BQBTZ** and ***m*-BQBTZ** at a heating rate of 10°C/min.

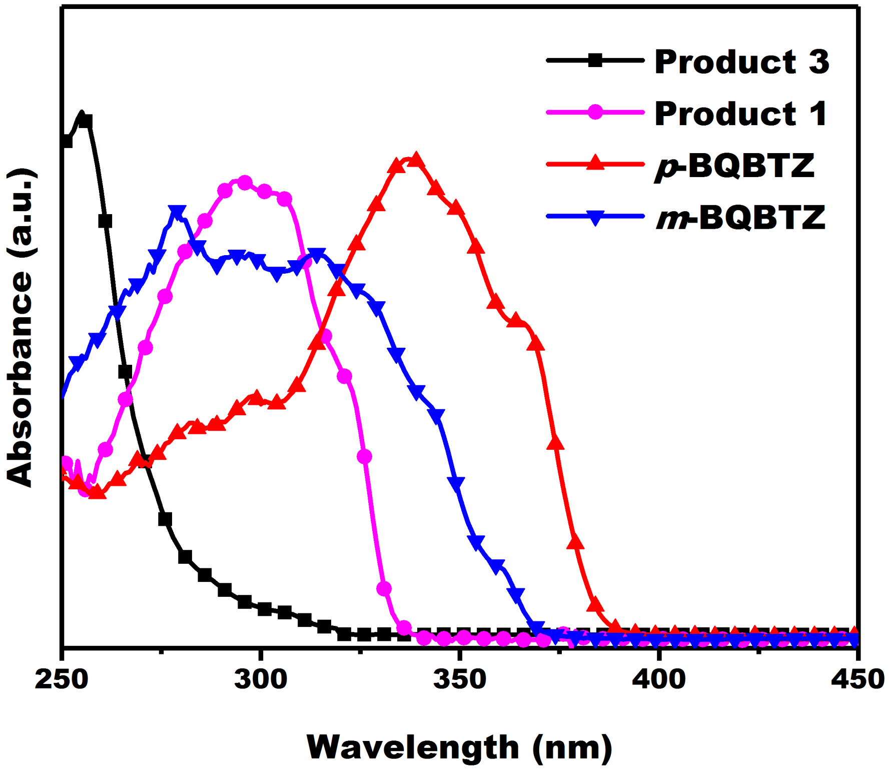

Figure S9. UV-visible absorption spectra of product 1, product 3, ***p*-BQBTZ** and ***m*-BQBTZ** in dilute THF solution.

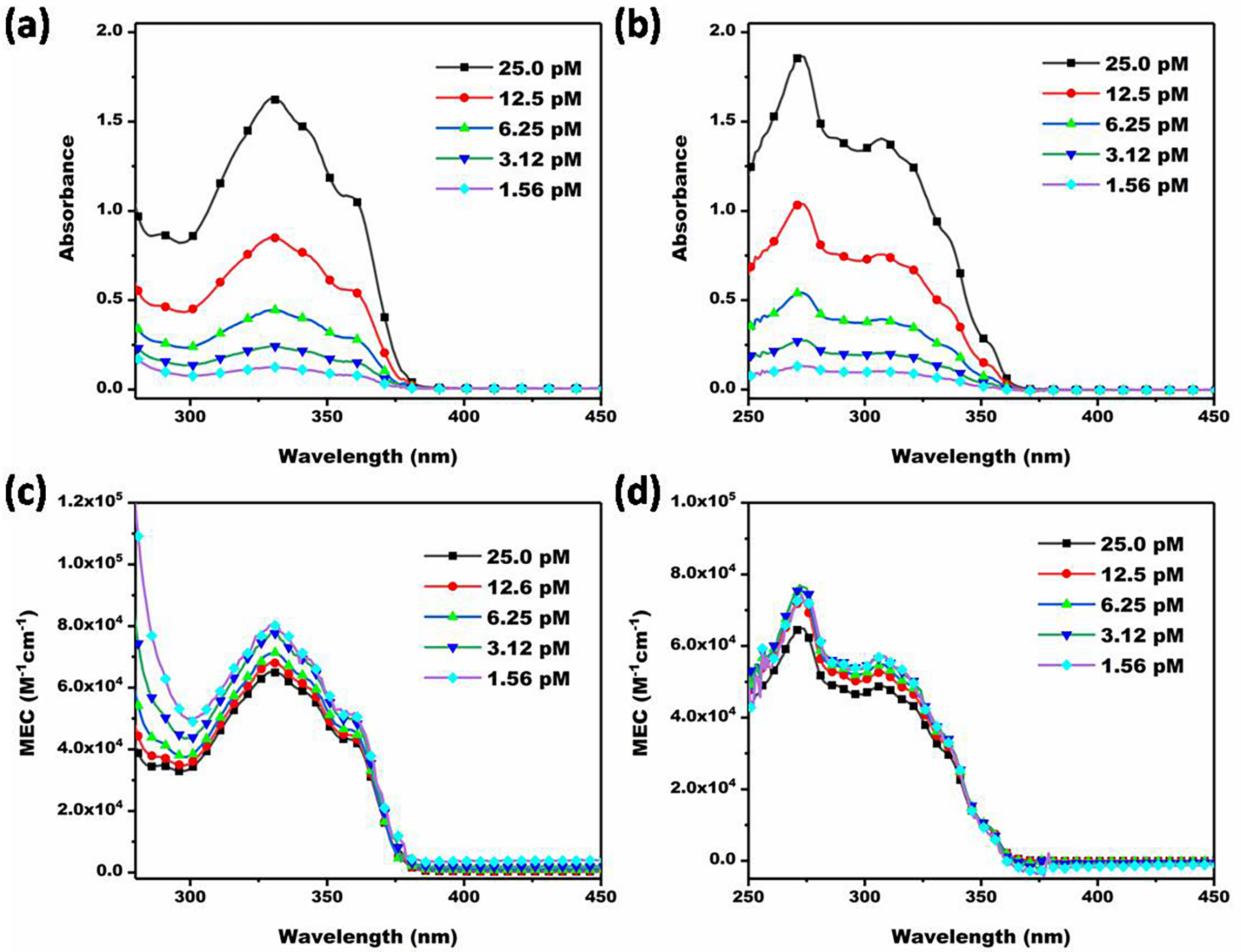

Figure S10. UV-visible absorption spectra of (a) ***p*-BQBTZ** and (b) ***m*-BQBTZ** in THF solution with different concentrations; molar extinction coefficients of (c) ***p*-BQBTZ** and (d) ***m*-BQBTZ** in THF solution with different concentrations.

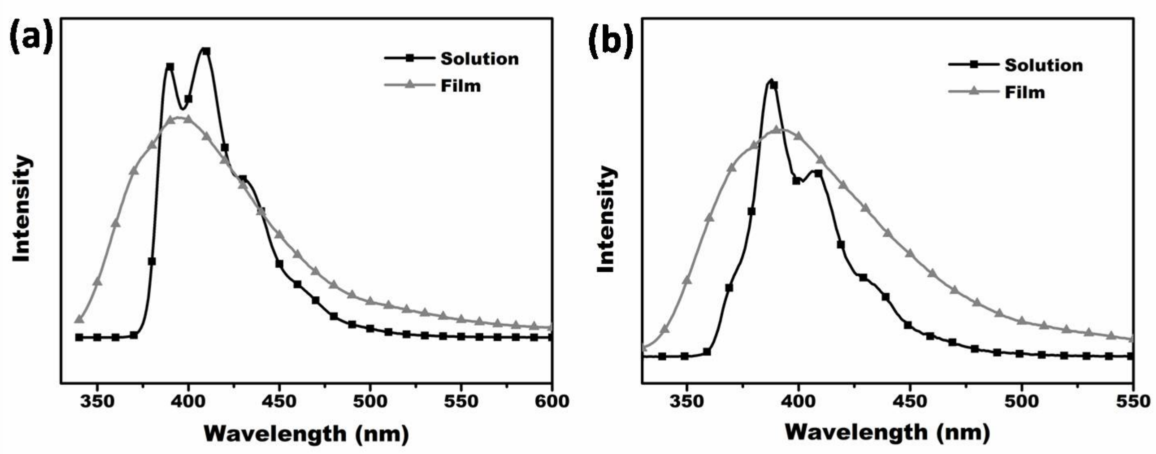

Figure S11. Fluorescence spectra of *p*-BQBTZ and *m*-BQBTZ in dilute THF solution and on films (a and b).

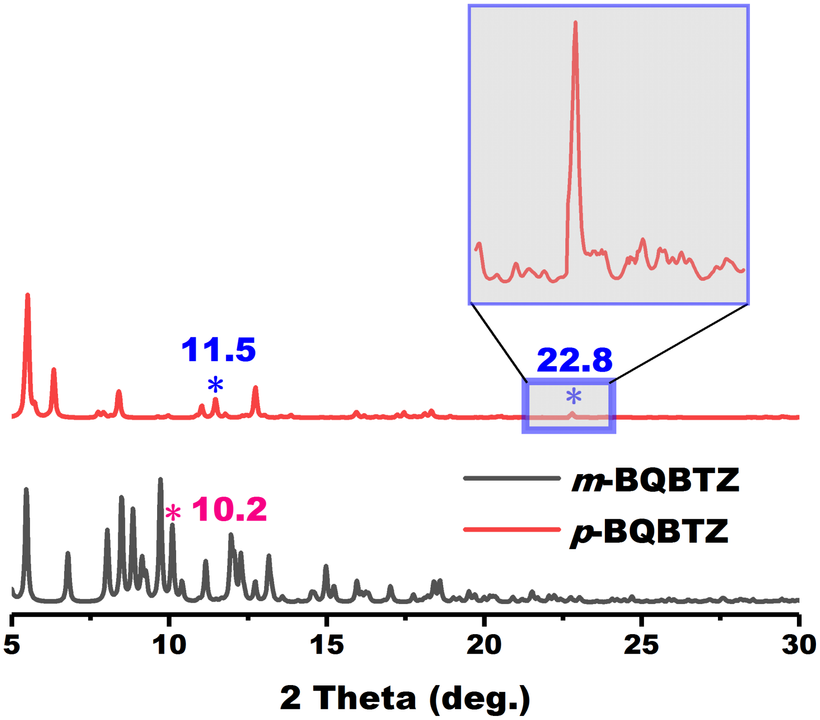

Figure S12. The simulated PXRD patterns of ***p*-BQBTZ** and ***m*-BQBTZ** packings.

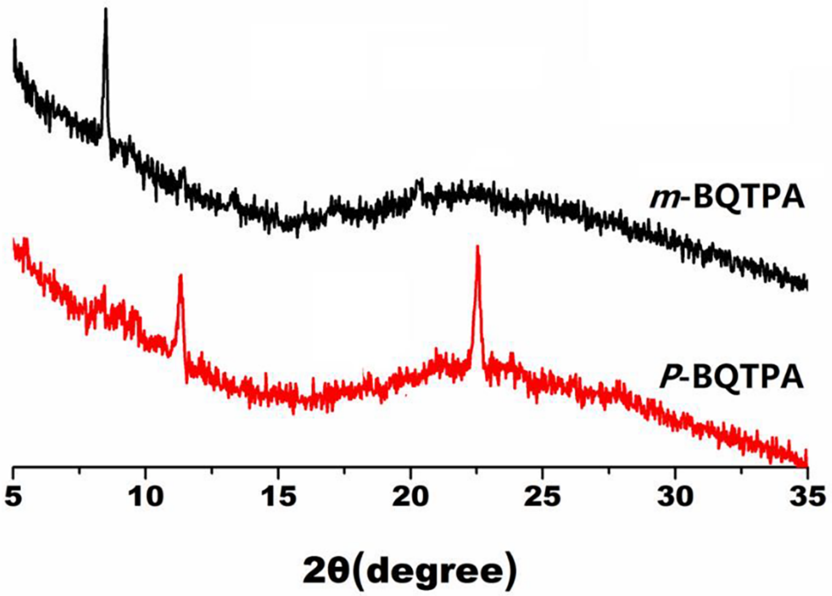

Figure S13. XRD patterns of the two thin films.

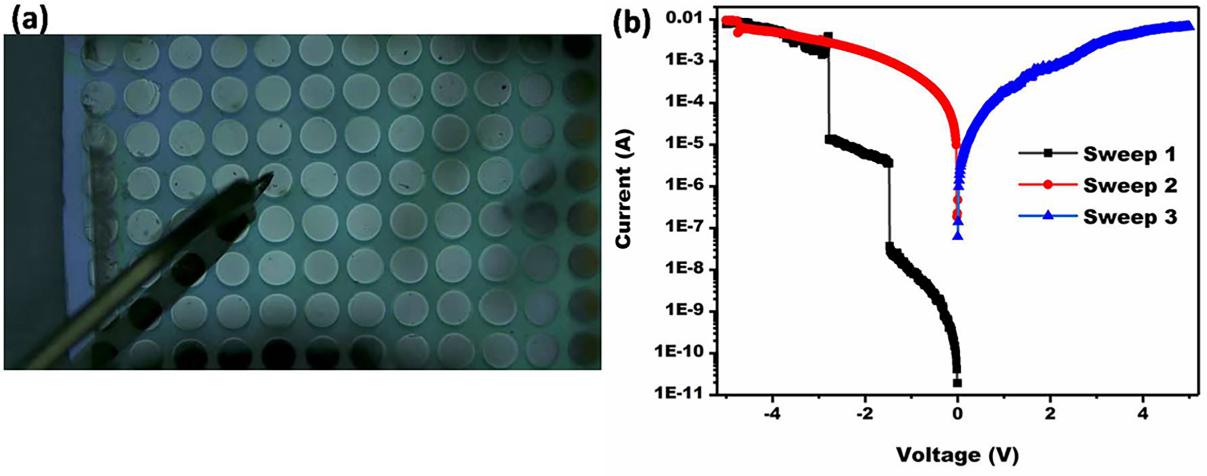

Figure S14. (a) The active device area was about 1.13 mm^2 using microscope; (b) Current-voltage (*I*–*V*) characteristics of ITO/*p*-**BQBTZ**/Al device.

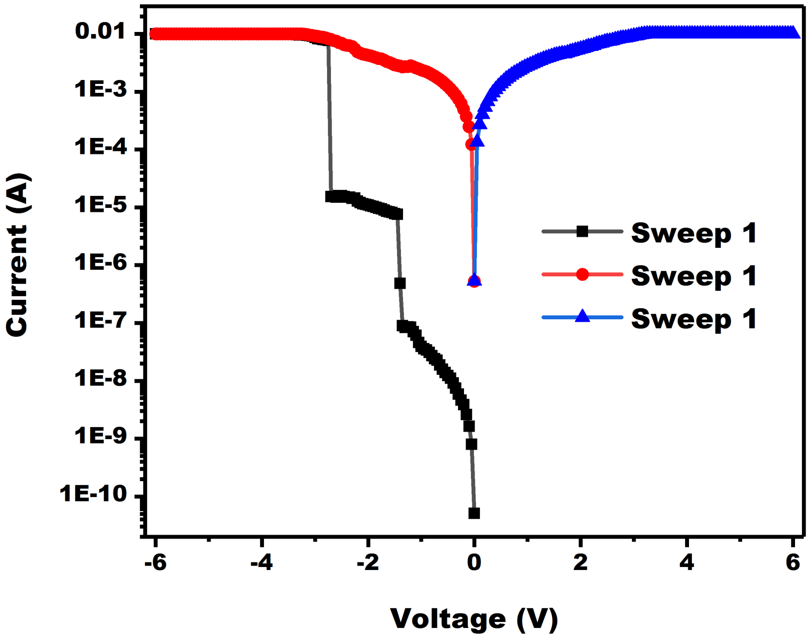

Figure S15. Current-voltage (*I*–*V*) characteristics of ITO/*p*-**BQBTZ**/LiF/Al device.

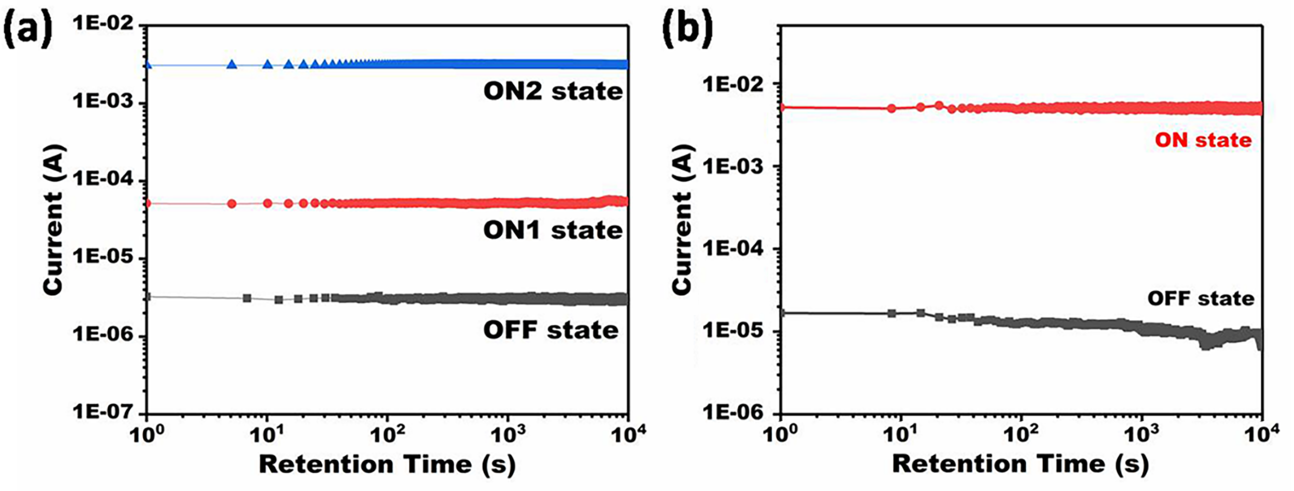

Figure S16. Stability test of (a) *p*-**BQBTZ** and (b) *m*-**BQBTZ** based memory devices in all states under stimulus by read pulses at -1 V.

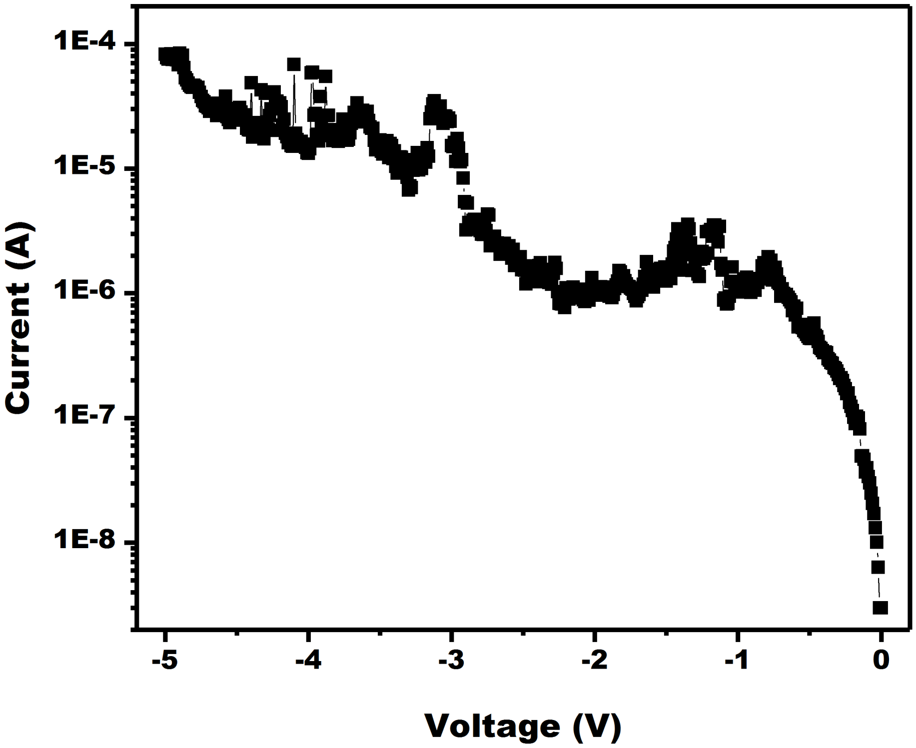

Figure S17. Current-voltage (*I*–*V*) characteristics of ***p*-BQBTZ** and ***m*-BQBTZ** based devices with no obvious memory behaviors.

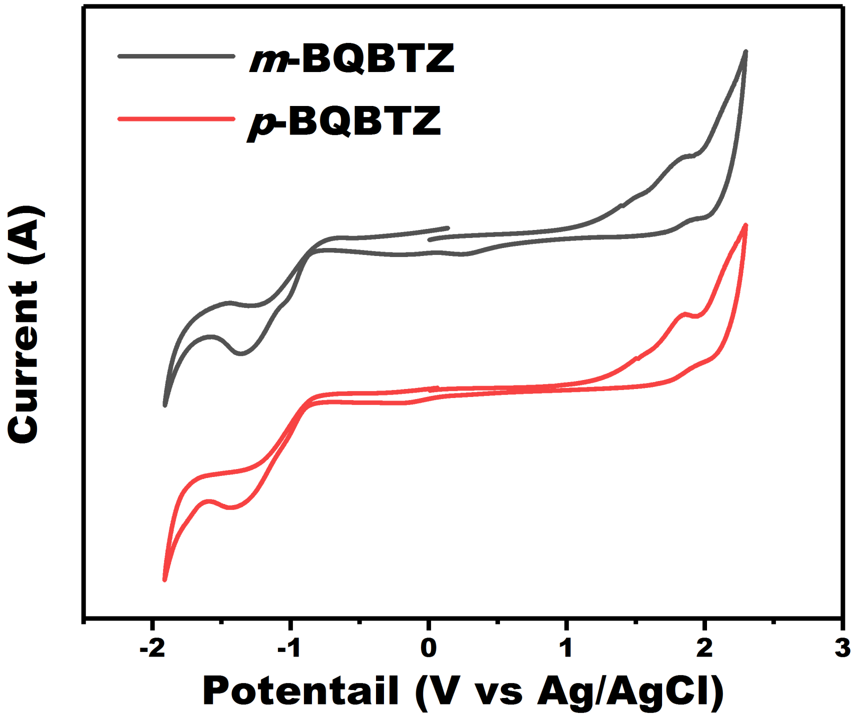

Figure S18. Cyclic voltammogram of *p*-BQBTZ and *m*-BQBTZ in CH_3CN with 0.1 M tetrabutylammonium perchlorate as electrolyte and ITO glass as the working electrode.

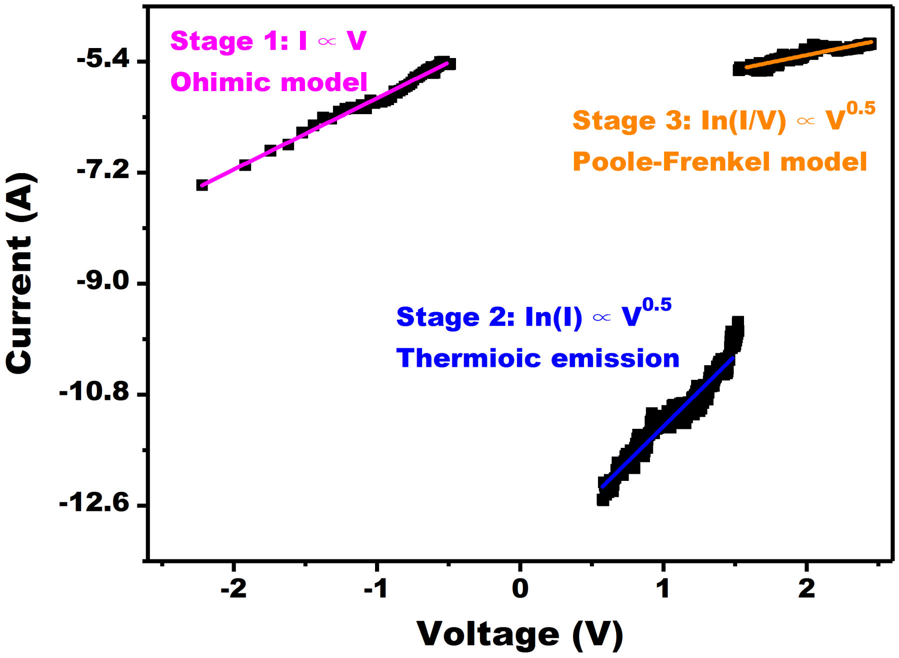

Figure S19. (a) The ohmic model at the first stage; (b) the thermionic emission model for stage 2; (c) the Poole–Frenkel emission model at the ON state, for stage 3.

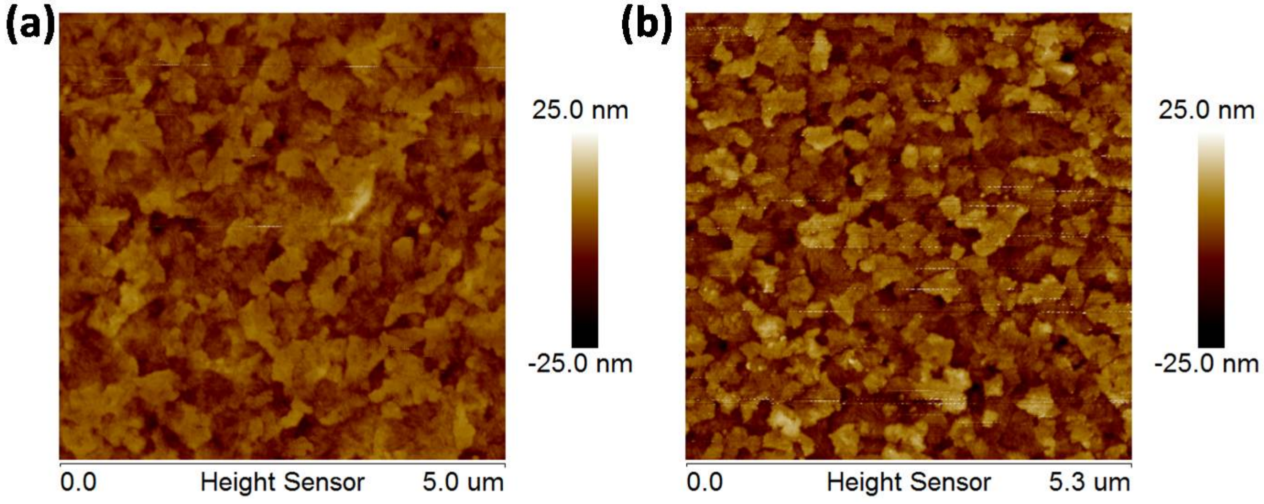

Figure S20. Tapping-mode AFM height images of the ***p*-BQBTZ** (a) and ***m*-BQBTZ** (b) on ITO substrate.

Table S1. Optical and electrochemical properties of the two synthesized molecules.

Compound	E_g/eV	HOMO/eV	LUMO[1]/eV	LUMO[2]/eV	HOMO (DFT)	LUMO (DFT)
p-BQBTZ	3.07	–5.28	–2.21	-3.44	-5.44	-2.14
m-BQBTZ	3.29	–5.33	–2.04	-3.42	-5.71	-1.93

5. Reference

(1) Wang XS, Li Q, Yao CS, Tu SJ, *Eur. J. Org. Chem.*, 2008, 20: 3513